# Effects of Thermal and Mechanical Fatigue on Flexural Strength of G40-600/PMR-15 Cross-Ply Laminates

GARY D. ROBERTS,*,[1] BARRY PING HSIAO HO,[2] and JOHN F. WALLACE[2]

[1]National Aeronautics and Space Administration, Lewis Research Center, Cleveland, Ohio 44135 and [2]Case Western Reserve University, Cleveland, Ohio 44106

## SYNOPSIS

The effects of thermal and mechanical fatigue on the flexural strength of G40-600/PMR-15 cross-ply laminates with ply orientations of $(0_2, 90_2)_{2S}$ and $(90_2, 0_2)_{2S}$ are examined. The relative importance of shear and tensile stresses is examined by varying the span-to-depth ratios of flexural test specimens from 8 to 45. Acoustic emission signals are measured during the flexural tests in order to monitor the initiation and growth of damage. Optical microscopy is used to examine specimens for resin cracking, delamination, and fiber breaks after testing. Transverse matrix cracks and delaminations occur in all specimens, regardless of ply orientation, span-to-depth ratio, or previous exposure of specimens to thermal and mechanical fatigue. A small amount of fiber tensile fracture occurs in the outer 0° ply of specimens with high span-to-depth ratios. Because of the complex failure modes, the flexural test results represent the "apparent" strengths rather than the true flexural or shear strengths for these cross-ply laminates. Thermal cycling of specimens prior to flexural testing does not reduce the apparent flexural strength or change the mode of failure. However, fewer acoustic events are recorded at all strains during flexural testing of specimens exposed to prior thermal cycling. High temperature thermal cycling (32–260°C, 100 cycles) causes a greater reduction in acoustic events than low temperature thermal cycling (−85 to 85°C, 500 cycles). Mechanical cycling (0–50% of the flexural strength, 100 cycles) has a similar effect, except that acoustic events are reduced only at strains less than the maximum strain applied during flexural fatigue. © 1994 John Wiley & Sons, Inc.[†]

## INTRODUCTION

High performance, polymer matrix composites (PMCs) are used in aeronautic and space applications because of their high stiffness and high strength-to-weight ratio. Because PMCs used in these applications are exposed to a wide range of temperatures, their service life is often limited by the damage formed during thermal cycling. In space applications, temperatures vary as an orbiting satellite moves in and out of Earth's shadow. In aircraft engine applications, rapid heating occurs during takeoff, and temperatures vary from ambient to about 300°C during flight. Microcracking induced by thermal cycling and oxidative degradation can be tolerated in engine applications as long as critical mechanical properties, such as compressive strength, are not degraded below acceptable limits. Although the performance advantages of PMCs have been demonstrated in military aircraft engines, use of PMCs in commercial aircraft engines is only recently being considered. Before PMCs can be used for load bearing structures in commercial engines, a better understanding of damage initiation and growth during thermal cycling is needed so that reliable models can be developed for predicting their service life. This information is also needed so that reliable test methods can be developed for evaluating new resins with improved resistance to damage induced by thermal cycling. Flexural tests are often used to evaluate new high temperature matrix resins and to study the degradation of composite properties after thermal cycling and high temperature isothermal

---

aging. Although the failure mode for PMCs in flexure is often complex, flexural tests are one of the few techniques that can be used to provide information about composite properties when limited amounts of material are available. The reliability and usefulness of flexural test data are improved if failure mechanisms are monitored during testing. Analysis of the acoustic signals emitted during mechanical deformation can provide information about the onset of damage and, in some cases, the type of failure (i.e., fiber tensile fracture, matrix cracking, fiber/matrix debonding). Acoustic emission data has provided useful information about the failure process for graphite/epoxy PMCs tested in tension, flexure, and fatigue,[1-5] but little information is available for high temperature polyimide matrix materials such as PMR-15. In this work, acoustic emission was recorded during three- and four-point flexure testing of graphite/PMR-15 cross-ply laminates. The effects of low temperature thermal cycling, high temperature thermal cycling, and mechanical cycling on the flexural strength and modes of failure were examined.

## EXPERIMENTAL

### Fabrication of Laminates and Test Specimens

The G40-600/PMR-15 prepreg used in this work was supplied by Ferro Corporation. The 16 plies of prepreg required for a $(0_2, 90_2)_{2S}$ layup were cut and stacked in a 15.2 × 30.5 cm (6 × 12 in.) tray with fibers in the outer plies aligned along the 30.5-cm (12-in.) length. A metal plate was placed on top of the stack to provide slight pressure. The tray was then placed in an oven at 204°C for 1 h to imidize the PMR-15 monomers. The imidized material was then placed in a tight fitting 15.2 × 30.5 cm (6 × 12 in.) mold and cured in a press under 500 psi pressure for 2 h at 316°C. The laminate was removed from the mold and postcured in an oven for 16 h at 316°C. The volume fraction of fibers measured by digestion of the matrix with sulfuric acid was 0.70. Laminates were C-scanned to verify that there were no delaminations present. Test specimens in the shape of rectangular beams were cut from the laminates using a water-cooled, diamond-impregnated cutting wheel. Beams cut parallel to the length of the laminate had fibers in the outer plies parallel to the beam length, or a $(0_2, 90_2)_{2S}$ layup. Beams cut perpendicular to the length of the laminate had fibers in the outer plies perpendicular to the beam length, or a $(90_2, 0_2)_{2S}$ layup. Edges of the beams were examined for

transverse cracking using an optical microscope. No cracks were visible on the cut edges of the beams prior to testing.

### Flexural Tests

Three- and four-point flexure tests were conducted according to the test procedure[6] described in ASTM D 790 using an Instron Model 1123 test machine. The three-point flexure specimens were 5.8 mm wide and 2.2 mm thick. Span lengths were set to provide span-to-depth ratios ranging from 8 to 45. Three specimens were tested at each span-to-depth ratio. Error bars are calculated as ±2 standard deviations (SD). The rate of cross-head displacement ranged from 0.25 to 5 mm/min in order to obtain an effective strain rate close to 0.01 min$^{-1}$ for the various span-to-depth ratios, as described in ASTM D 790. Four-point flexure specimens were 5.8 mm wide, 2.2 mm thick, and 120 mm long. A span-to-depth ratio of 45 and a deflection rate of 5 mm/min were used for all four-point bend tests. The load span was one half the support span.

According to the ASTM D 790 test procedure, the maximum strain at failure in the outer ply of the laminate can be calculated for three- and four-point bend tests using eqs. (1) and (2),

$$r = 6Dd/L^2 \quad \text{(three-point bend)} \quad (1)$$

$$r = 4.36Dd/L^2 \quad \text{(four-point bend)} \quad (2)$$

and the apparent flexural strength can be calculated using eqs. (3) and (4).

$$S = 3PL/2bd^2 \quad \text{(three-point bend)} \quad (3)$$

$$S = 3PL/4bd^2 \quad \text{(four-point bend)} \quad (4)$$

where $D$ is midspan deflection, $L$ is support span, $d$ is depth of beam, $b$ is width of beam, and $P$ is applied load. A procedure for measuring the apparent interlaminar shear strength of composite beams with low span-to-depth ratios is described in ASTM D 2344.[7] According to this test procedure, the apparent interlaminar shear strength of three-point bend specimens can be calculated using eq. (5).

$$S = 0.75P/bd. \quad (5)$$

Several limitations exist on the use of eqs. (1)–(5) for the cross-ply laminates investigated in this work. The applicability of these equations is discussed below along with the test results.

## Thermal and Mechanical Cycling

Flexural test specimens were exposed to low temperature thermal cycling, high temperature thermal cycling, mechanical cycling, and combined low temperature thermal cycling followed by mechanical cycling. For low temperature cycling, specimens were placed in a cylindrical sample holder and locked into an air actuated piston. The specimens were then cycled 500 times between a chamber heated to 85°C and a chamber cooled to −85°C. The heating rate was estimated to be about 60°C/min, and the cooling rate was estimated to be about 100°C/min. High temperature thermal cycling was conducted using a MOEN HT251 thermal cycler made by Heat Transfer Technologies, Inc. The specimens were suspended in racks placed inside the thermal cycling unit. The temperature was then cycled between 32 and 260°C for 100 cycles. The heating ramp was linear with a heating rate of 26.7°C/min (80°F/min). The maximum cooling rate was 32.8°C/min (91°F/min) at the beginning of the cooling cycle, but the cooling rate decreased steadily throughout the cycle. Mechanical cycling was conducted using four-point bend specimens deformed to 50% of the fracture load for 100 cycles at a deflection rate of 5 mm/min.

## Acoustic Emission Detection

A NANO 30 acoustic sensor was attached to the specimens to monitor acoustic events during the flexural tests. High vacuum silicone grease was used as a coupling medium. The acoustic sensor was connected to a 40-dB gain preamplifier with a resonant frequency of 300 kHz. A cable delivered the data from the preamplifier to a SPARTAN AT data analyzer made by Physical Acoustics Corporation with a threshold gain of 26 dB. These test parameters have been shown by previous studies to provide the best behavior information.

## RESULTS AND DISCUSSION

### Three-Point Bend Test Results

Typical load-deflection curves for the $(0_2, 90_2)_{2S}$ specimens are shown in Figure 1. Different deflection rates were used for different span-to-depth ratios, as specified in ASTM D 790. The acoustic events recorded during deformation are shown in Figure 2. Similar data are shown in Figures 3 and 4 for the $(90_2, 0_2)_{2S}$ specimens. The flexural strain (i.e., the maximum tensile strain in the outer ply) can be
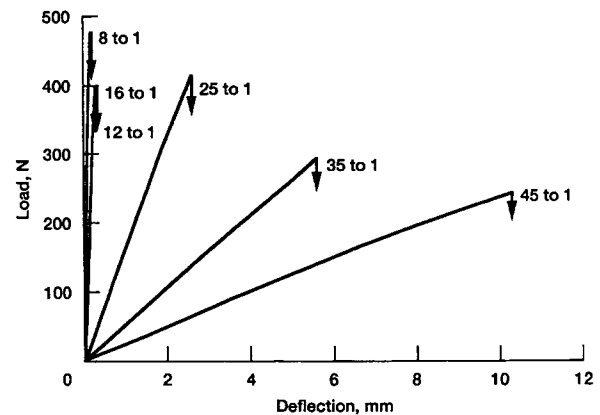


**Figure 1**   Load-deflection curves for $(0_2, 90_2)_{2S}$ specimens tested in three-point bending. Deflection rates (in mm/min) used for the various span/depth ratios are: 5 for 45/1, 4 for 35/1, 2 for 25/1, 1 for 16/1, 0.5 for 12/1, and 0.25 for 8/1.

calculated using eq. (1). The deflections corresponding to a strain of $r = 0.01$ are indicated as arrows in Figures 2 and 4. At low strains, the load-deflection curves are linear, and few acoustic events are recorded. At higher strains, the slopes of the load-deflection curves decrease, and the acoustic events increase until failure. Acoustic events begin at lower strains for specimens with higher span-to-depth ratios. In Figure 2, for example, acoustic events begin to increase at a strain of 0.002 when the span-to-depth ratio is 45 and at a strain of 0.006 when the span-to-depth ratio is 8.

Because the maximum strain at failure is less than 0.02 for all span-to-depth ratios, beam strengths are calculated according to eq. (3), which includes no correction for large deflections. Strengths calculated according to eq. (3) represent true flexural strengths only at high span-to-depth ratios and only when failure occurs in the outer fibers. In addition, eq. (3) is strictly valid only for homogeneous, elastic beams with linear load-deflection curves. Because these conditions are not satisfied for the graphite/PMR-15 cross-ply laminates used in this work, flexural strengths calculated according to eq. (3) are called "apparent" strengths, in accordance with the terminology in the ASTM D 790 test procedure. Apparent flexural strengths are shown as a function of span-to-depth ratio in Figure 5. Ideally, tensile failure should occur in the outer ply at high span-to-depth ratios and interlaminar separation should occur near the center plane at low span-to-depth ratios. However, the actual failure modes were more complex. Vertical cracks were present in all 90° plies, regardless of layup or span-
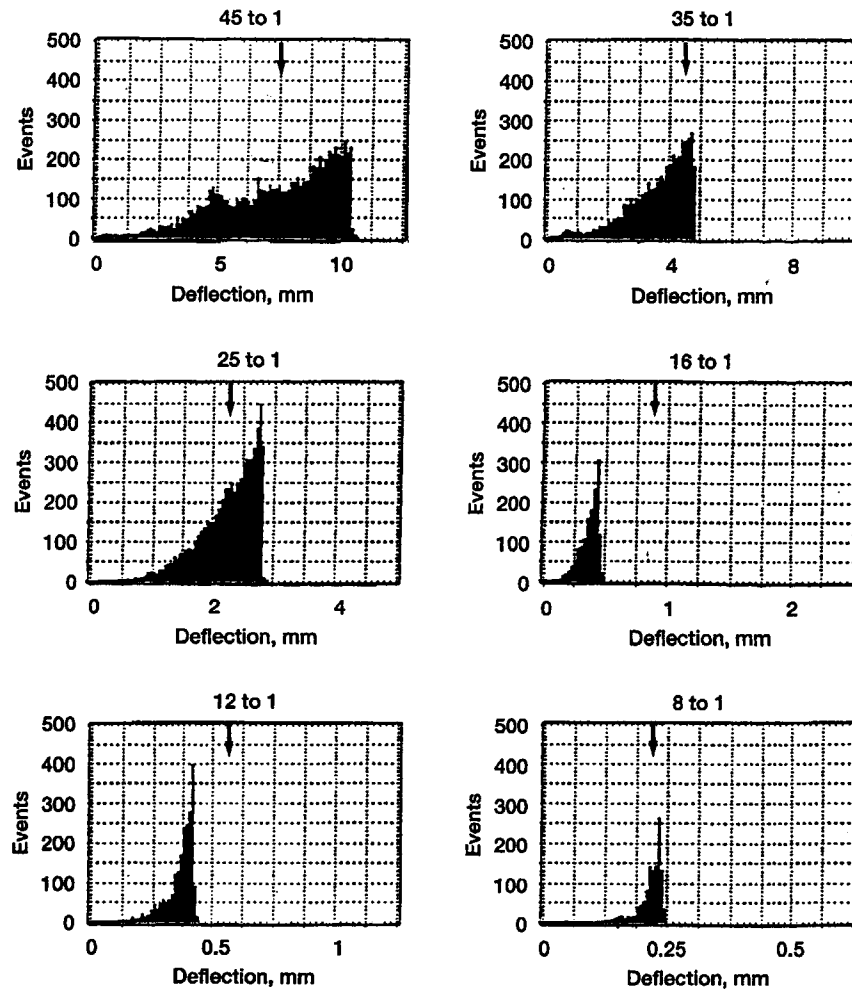
**Figure 2**   Acoustic events versus deflection for load-deflection curves shown in Figure 1. Arrows correspond to a strain of $r = 0.01$ calculated using eq. (1).
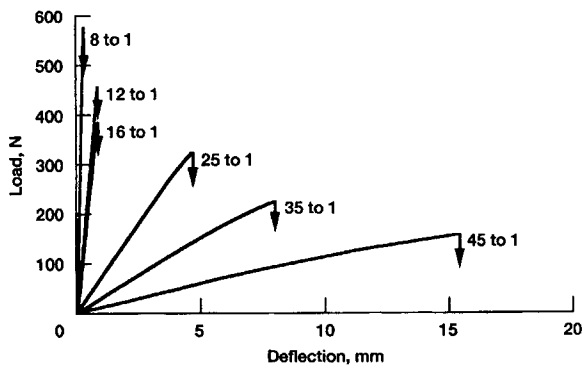


**Figure 3**   Load-deflection curves for $(90_2, 0_2)_{2S}$ specimens tested in three-point bending. Deflection rates (in mm/min) used for the various span/depth ratios are: 5 for 45/1, 4 for 35/1, 2 for 25/1, 1 for 16/1, 0.5 for 12/1, and 0.25 for 8/1.

to-depth ratio. These transverse cracks were not concentrated in the vicinity of the load point. Other features of the failure process depended on the span-to-depth ratio. These are described below.

The various types of failure observed on the beam edges after three-point bend testing are shown in Figure 6(a)-(d). The darker plies are the 90° plies. The 16 plies are numbered in Figure 6(a) to help locate features in the micrographs. At span-to-depth ratios of 16 and less, a single delamination occurred near the center of the beam, but the fracture surface was not confined to a single 0°/90° interface. Instead, the delamination sometimes crossed from one interface to another through the 90° plies. This usually occurred at the site of a vertical crack or at a 45° crack located near a vertical crack. For $(90_2, 0_2)_{2S}$ specimens, delamination alternated between
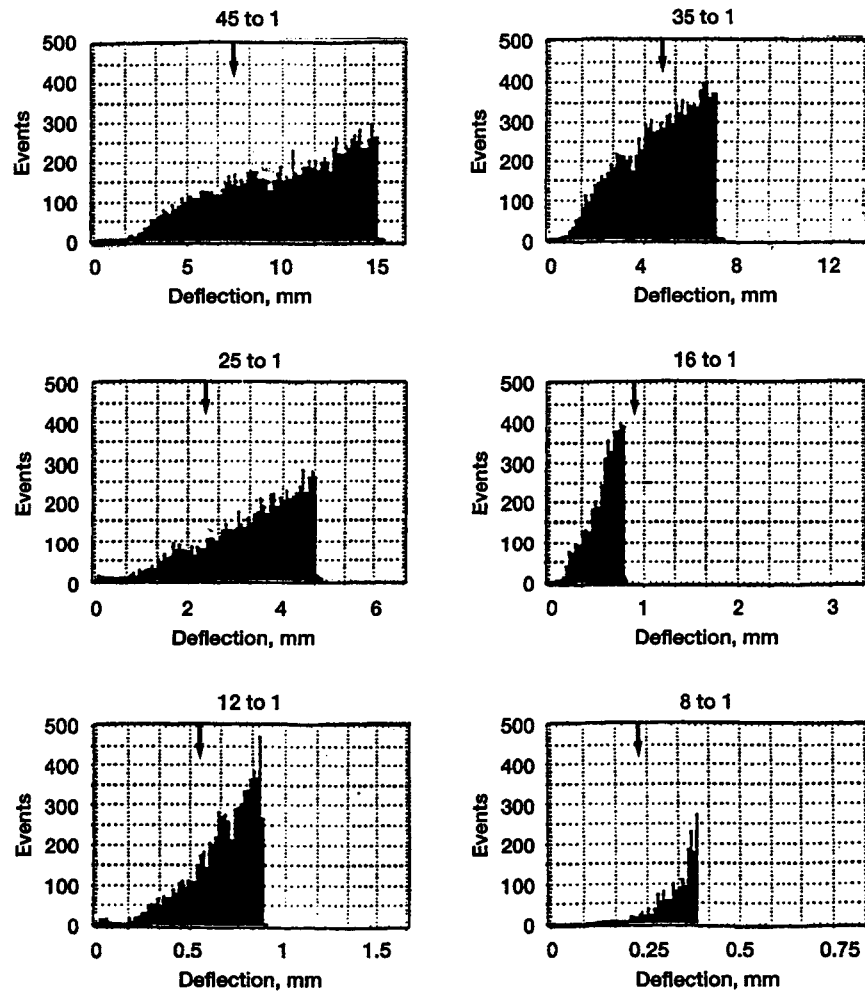
**45 to 1**

Events
500
400
300
200
100
0
0    5    10    15
Deflection, mm

**35 to 1**

Events
500
400
300
200
100
0
0    4    8    12
Deflection, mm

**25 to 1**

Events
500
400
300
200
100
0
0    2    4    6
Deflection, mm

**16 to 1**

Events
500
400
300
200
100
0
0    1    2    3
Deflection, mm

**12 to 1**

Events
500
400
300
200
100
0
0    0.5    1    1.5
Deflection, mm

**8 to 1**

Events
500
400
300
200
100
0
0    0.25    0.5    0.75
Deflection, mm

**Figure 4**   Acoustic events versus deflection for load-deflection curves shown in Figure 3. Arrows correspond to a strain of $r = 0.01$ calculated using eq. (1).

the 4/5 interface and the 6/7 interface. This type of failure is shown in Figure 6(a) for a $(90_2, 0_2)_{2S}$ specimen with a span-to-depth ratio of 8. The delamination starts on the left at the 4/5 interface, crosses through plies 5 and 6 at a 45° angle, then continues to the right along the 7/8 interface. For $(0_2, 90_2)_{2S}$ specimens, four 90° plies are at the center of the beam. Delamination alternated between the 6/7 and the 10/11 interfaces on either side of the central 90° plies.

At span-to-depth ratios of 25 and greater, transverse cracks and multiple delaminations occurred for both $(0_2, 90_2)_{2S}$ and $(90_2, 0_2)_{2S}$ specimens [Fig. 6(b)]. For $(0_2, 90_2)_{2S}$ specimens, some broken fibers were visible at the edge of the bottom ply (ply 1) but not across the entire bottom surface [Fig. 6(c)]. The number of broken fibers increased as span-to-

depth ratio increased from 25 to 45. For $(90_2, 0_2)_{2S}$ specimens, some fiber breaks were visible in the outermost 0° ply (ply 3) at locations where transverse cracks penetrated the outer 90° plies (plies 1 and 2). For both $(0_2, 90_2)_{2S}$ and $(90_2, 0_2)_{2S}$ specimens, fiber buckling occurred on the upper beam surface [Fig. 6(d)].

The acoustic events recorded during deformation clearly indicate that damage begins to accumulate long before failure. However, it was not possible to determine directly from the acoustic data what type of damage had occurred because the amplitude distribution of the events was broad with no clearly defined peaks corresponding to the various possible failure events. It is also not clear whether the damage observed by post failure analysis occurred before or after initiation of catastrophic failure. Some infor-
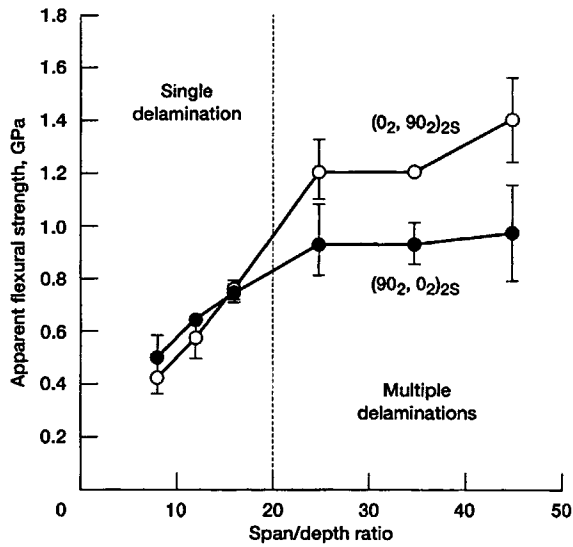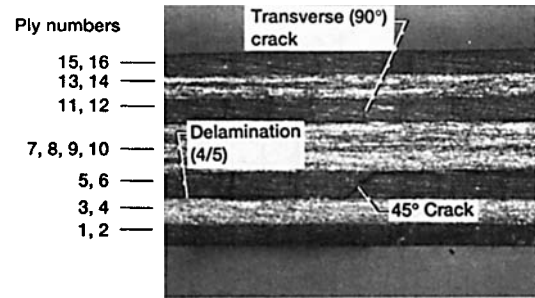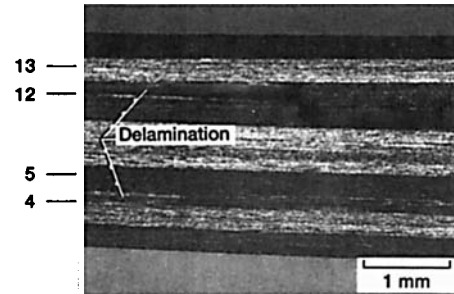
**Figure 5**  Apparent flexural strength of $(0_2, 90_2)_{2S}$ and $(90_2, 0_2)_{2S}$ laminates tested in three-point bending.



(a) $(90_2, 0_2)_{2S}$, S/D = 8.



(b) $(90_2, 0_2)_{2S}$, S/D = 45.



(c) $(0_2, 90_2)_{2S}$, S/D = 35.



(d) $(0_2, 90_2)_{2S}$, S/D = 45.

mation can be inferred from the magnitude of the strain in the outer ply at failure. For the $(0_2, 90_2)_{2S}$ specimens with a span-to-depth ratio of 45, the failure strain calculated using eq. (1) is 0.014. This is close to the fiber failure strain of 0.0144 measured by the prepreg manufacturer for fibers used in this particular lot of prepreg. As the span-to-depth ratio of the $(0_2, 90_2)_{2S}$ specimens decreases from 45 to 25, the calculated strain at failure decreases only slightly from 0.014. This suggests that flexural strength is determined by fiber tensile strength for $(0_2, 90_2)_{2S}$ specimens with high span-to-depth ratios and that damage which accumulates prior to failure has little effect on the apparent flexural strength. For all other specimens, failure is a complex process involving matrix cracking, transverse ply cracking, delamination, and possibly fiber breakage.
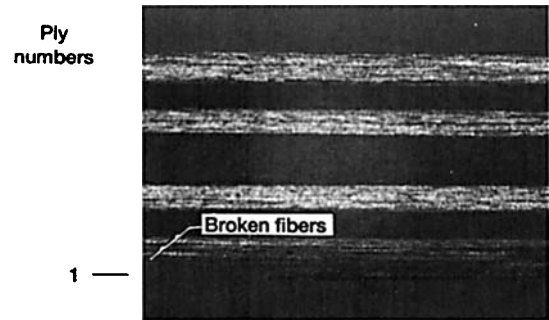
The strength of specimens with low span-to-depth ratios is often reported as the interlaminar shear strength (or the short beam shear strength) rather than the flexural strength. A procedure for calculating the apparent interlaminar shear strength of parallel fiber reinforced laminates by applying classical beam theory to short-beam shear specimens is described in ASTM D 2344.[7] This test method is limited to parallel fiber reinforced specimens with span-to-depth ratios of 4 or 5, and a warning is included in the test procedure that results are meant to be used only for comparative studies and not for generating design data. Interlaminar shear test data measured on graphite/epoxy specimens with various
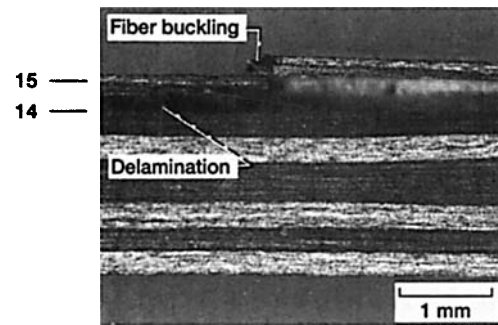
**Figure 6**  Failure modes observed by post-failure analysis of three-point bend specimens with ply layups of $(0_2, 90_2)_{2S}$ and $(90_2, 0_2)_{2S}$ and various span-to-depth ratios.

ply configurations and span-to-depth ratios as high as 16 has been reviewed by Whitney et al.[8,9] They concluded that combined compression and shear stresses lead to complex failure modes which limit the usefulness of the test, even for comparative studies. The primary problem is that vertical cracks are formed prior to failure and that the vertical cracks appear to be required to induce delamination. In spite of the limitations of the test method for accurately measuring interlaminar shear strength, the short beam shear test can be useful for assessing the initial quality of a laminate and the degradative effects of environmental exposure. For example, the short beam shear strength will be low if fiber/matrix bonding is poor or if matrix and interface properties have been degraded by exposure of the laminate to high temperatures or thermal cycling. Apparent interlaminar shear strengths of the graphite/PMR-15 specimens are shown in Figure 7. Note that Figures 5 and 7 represent the same test data calculated in two different ways [i.e., using eq. (3) for flexural strength and eq. (5) for shear strength]. If shear strengths calculated according to eq. (5) were valid, the shear strengths in Figure 7 should approach a constant value at low span-to-depth ratios. This is not the case for either the $(0_2, 90_2)_{2S}$ or the $(90_2, 0_2)_{2S}$ specimens. Although accurate interlaminar shear strengths cannot be determined from the data of Figure 7, it does appear that the $(90_2, 0_2)_{2S}$ specimens are stronger than the $(0_2, 90_2)_{2S}$ specimens
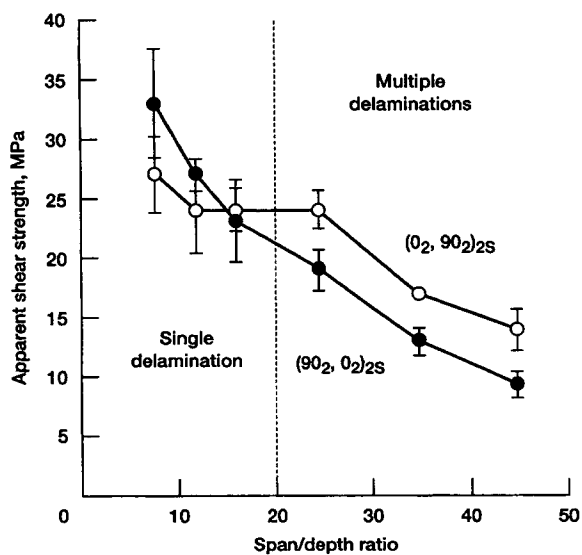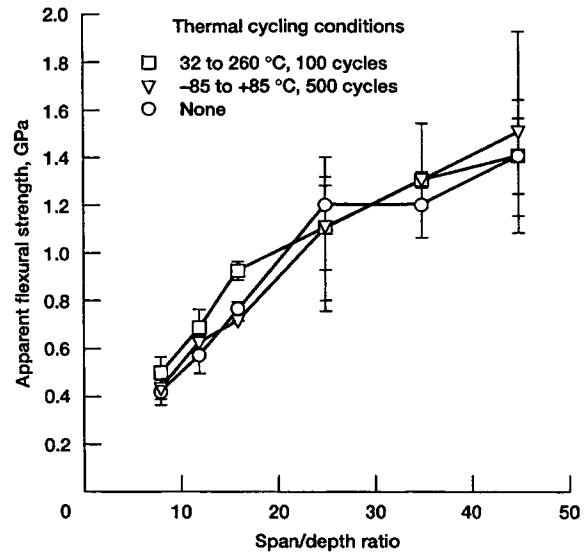


**Figure 8**  Effect of thermal cycling on the apparent flexural strength of $(0_2, 90_2)_{2S}$ specimens tested in three-point bending.

at low span-to-depth ratios. Because the $(0_2, 90_2)_{2S}$ and $(90_2, 0_2)_{2S}$ specimens were cut from the same laminate, the difference in strength must be a result of the ply stacking sequence and the location of failure rather than a difference in the actual interlaminar shear strength between the 0° and 90° plies.

Because measurements at low span-to-depth ratios do not appear to represent the true interlaminar shear strength, the effects of thermal cycling on the three-point bend data will be presented only in the form of apparent flexural strength. Low temperature cycling (−85 to 85°C for 500 cycles) was used to simulate thermal loads experienced by satellites in low Earth orbit. High temperature cycling (32–260°C for 100 cycles) was used to simulate service conditions for polymer matrix composites in aircraft gas turbine engines. The effect of thermal cycling on the strengths of $(0_2, 90_2)_{2S}$ and $(90_2, 0_2)_{2S}$ specimens is shown in Figures 8 and 9. The failure modes for the uncycled specimens were described above. Thermal cycling had little effect on either the failure modes or the apparent flexural strength. The total number of acoustic events accumulated during deformation was smaller for specimens that had been thermally cycled, with high temperature cycling resulting in a larger reduction in total events. The number of events is lower for the thermally cycled materials because some of the damage that would have been induced during the test by mechanical loading has already occurred during thermal cycling.
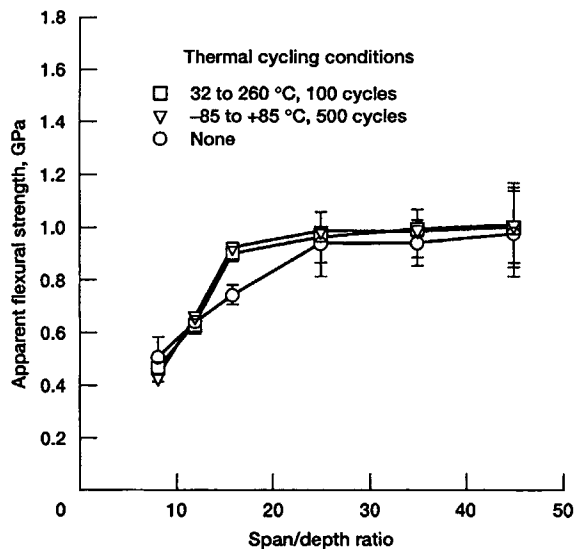


**Figure 7**  Apparent interlaminar shear strength of $(0_2, 90_2)_{2S}$ and $(90_2, 0_2)_{2S}$ laminates tested in three-point bending.

**Figure 9**   Effect of thermal cycling on the apparent flexural strength of $(90_2, 0_2)_{2S}$ specimens tested in three-point bending.

The distance between transverse cracks in the $90°$ plies varied from specimen to specimen and from ply to ply within a given specimen. However, the density of transverse cracks at the site of maximum crack density was nearly the same (approximately two cracks/mm) for all specimens, regardless of thermal history. For $(0_2, 90_2)_{2S}$ laminates, the maximum crack density occurred in the $90°$ plies adjacent to the outer $0°$ plies (plies 3 and 4). For the $(90_2, 0_2)_{2S}$ laminates, the maximum crack density occurred in the $90°$ plies adjacent to the center $0°$ plies (plies 5, 6, 11, and 12).

Two additional sets of three-point bend experiments were conducted in order to examine the growth of damage prior to failure. First, acoustic events were monitored for specimens held under high static loads in order to determine whether stress relaxation and time dependent failure in the matrix were significant. A $(0_2, 90_2)_{2S}$ specimen with a span-to-depth ratio of 45 was deformed to 70% of the expected failure load. The specimen was then held at constant deflection for 35 min before the deflection was continued. During the hold at constant deflection, the load remained constant, and only a few acoustic events occurred. The deflection was then continued until the specimen failed. The load at failure was not affected by application of the static load. Similar results were obtained for lower static loads and for $(90_2, 0_2)_{2S}$ specimens. This indicates that time dependent effects are not significant for the room temperature tests. In a second set of ex-

periments, $(0_2, 90_2)_{2S}$ specimens with a span-to-depth ratio of 45 were loaded and unloaded in a single cycle with maximum loads of 10, 30, 50, 70, and 90% of the expected failure load. After the loading cycle, the specimens were cut in half by making a vertical cut along the length of the specimens. The pieces were then examined for cracks on both the original outer edge of the specimen and on the interior edge of the specimen exposed by cutting. Only a few cracks were observed on the outer edges, even after loading to 90% of the breaking load. However, cracks were observed on the interior edge with the maximum crack density located near the load point. The maximum crack density in the interior was much lower than the maximum edge crack density reported above (2 cracks/mm) for specimens loaded to failure. The density of interior cracks was not strongly affected by the magnitude of the applied load. This appears to be in conflict with the data of Figure 2, in which the number of acoustic events increases steadily as the load is increased. However, it is probable that some of the failure events are too small to be visible by optical microscopy at low magnifications. Examination of selected specimens at magnifications up to 500 times did reveal smaller cracks that did not cross an entire ply. Tomkins and Williams[10] have noted that the extent of micro-cracking in Celion 6000/PMR-15 laminates could be determined better by x-ray than by optical microscopy. Further work, including x-radiography, is needed to determine the type and location of damage that occurs at various strains during flexure testing of the G40-600/PMR-15 laminates. Because a single acoustic detector was used to obtain the data of Figures 2 and 4, it was not possible to determine the location of the acoustic events recorded at various times during the load-deflection cycle. Further experiments using two detectors would be useful for determining whether damage induced at low strains is concentrated near the load point.

## Four-Point Bend Tests

As mentioned above, the ideal failure mode for flexural specimens with high span-to-depth ratios is fiber tensile failure in the outer ply at the location of maximum tensile stress. For three-point bend specimens, the region of maximum tensile stress is located directly under the load point. However, significant shear stresses are also present in this region. For four-point bend specimens, the region of maximum tensile stress is located between the load points where the specimen is deformed in a pure

bending mode. Because the shear stress is zero in pure bending, failure analysis is simplified for four-point bend tests if failure occurs between the load points. Outside of this region (i.e., in the region between the load points and the support points) the shear stress is nonzero. For specimens with the same span-to-depth ratio, the load required to produce a particular value of the maximum tensile stress in a four-point bend test is twice that required in a three-point bend test [eqs. (3) and (4)]. At equal values of the maximum tensile stress, the maximum shear stress in the four-point bend test is twice that in the three-point bend test.[11] Although this analysis is based on simple beam theory, the shear stress for composite specimens will still be higher in the four-point bend test than in the three-point bend test as long as the specimens have the same ply layup. As a result, specimens that fail in flexure during a three-point bend test may fail in shear during a four-point bend test.

Four-point bend tests were done using $(0_2, 90_2)_{2S}$ and $(90_2, 0_2)_{2S}$ specimens with a span-to-depth ratio of 45. The effects of low temperature thermal cycling ($-85$ to $85°C$ for 500 cycles), mechanical cycling (50% of fracture load for 100 cycles), and combined cycling (500 low temperature thermal cycles followed by 100 mechanical cycles) were examined. For $(0_2, 90_2)_{2S}$ specimens, extensive transverse cracking was present in all $90°$ plies after the flexure tests. Multiple delaminations occurred primarily at $0°/90°$ interfaces in the middle and top portions of the beams. Compressive failures were located on the top surface for only two of the specimens. One of these was near a load point, and the other between the load points. For $(90_2, 0_2)_{2S}$ specimens, transverse cracks also occurred in all $90°$ plies. Total delaminations were located between the top $0°$ ply and the $90°$ ply below it. Some localized delamination also occurred between other plies. No broken fibers were observed for either $(0_2, 90_2)_{2S}$ or $(90_2, 0_2)_{2S}$ specimens. Apparent flexural strengths are shown in Table I. The flexural strengths in Table I are lower than those shown in Figure 5 for the three-point bend specimens with a span-to-depth ratio of 45. The severe delamination, the lack of broken fibers, and the lower apparent flexural strengths for the four-point bend specimens indicate that shear induced delamination occurred before the tensile stress became large enough to break the fibers in the outer ply.

The data of Table I indicate that thermal, mechanical, and combined cycling have little effect on the apparent flexural strengths. Acoustic events re-

**Table I   Effects of Thermal and Mechanical Cycling on Apparent Flexural Strength of Four-Point Bend Specimens With a Span-to-Depth Ratio of 45**

| Specimen | Apparent Flexural Strength (GPa) | |
|---|---|---|
| | $(0_2, 90_2)_{2S}$ | $(90_2, 0_2)_{2S}$ |
| No cycling | 1.0 | 0.69 |
| Thermal cycling | 1.1 | 0.69 |
| Mechanical cycling | 1.0 | 0.69 |
| Thermal and mechanical cycling | 1.0 | 0.71 |

corded during testing are shown in Figures 10 and 11. Although strength is not reduced by thermal and mechanical cycling individually or combined, the number of acoustic events recorded during subsequent testing is reduced. Thermal cycling reduces the number of events recorded at all strains. Mechanical cycling eliminates acoustic events at low strains, but has little effect at higher strains. These results are reasonable because thermal cycling causes damage throughout the specimen, and mechanical cycling causes damage only in regions where damage would normally occur during the first half of the flexural test. The acoustic events recorded during mechanical cycling are shown in Figure 12 for specimens with no prior thermal cycling and in Figure 13 for specimens with prior thermal cycling. Most of the damage occurs during the first mechanical cycle. Acoustic events that occur after the first cycle could be caused by further damage or by friction between the surfaces formed by previous damage. Friction has been found to be a major source of acoustic emission during tension fatigue testing of cross-ply laminates.[1] If the acoustic events recorded during flexural loading were associated with friction, the number of events should increase as the extent of damage is increased by thermal or mechanical cycling. However, the data in Figures 12 and 13 indicate that both thermal and mechanical cycling reduce the number of events. The acoustic events recorded during mechanical cycling are therefore caused by further damage rather than by friction. The absence of friction related events is consistent with the observation of transverse cracking as the dominant subcritical damage mode because the cracks will open and close during mechanical cycling with no sliding (or friction) between the fracture surfaces.
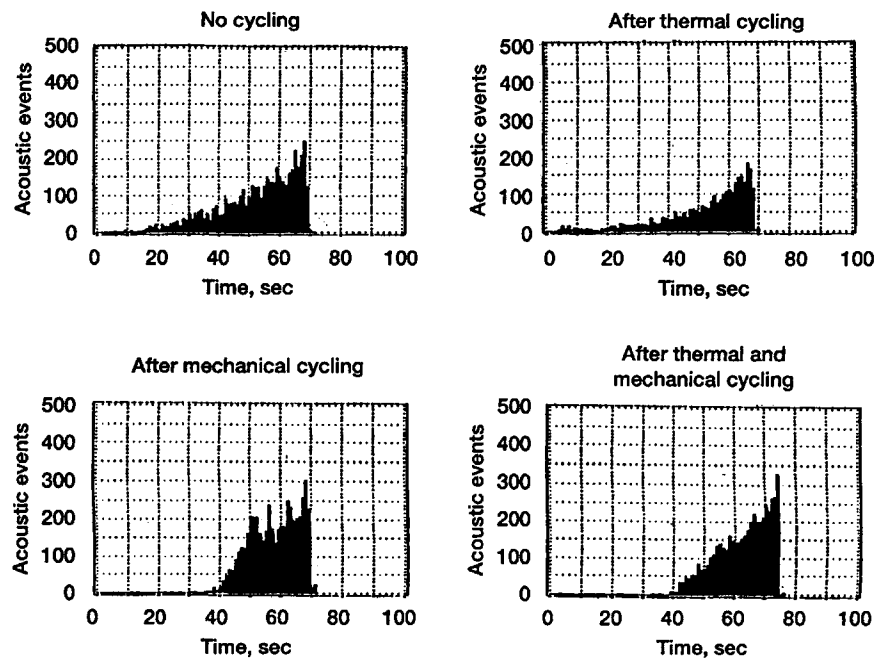
**Figure 10** Effect of low temperature thermal cycling and mechanical cycling on acoustic events recording during four-point bend testing of $(0_2, 90_2)_{2s}$ specimens with a 45/1 span/ depth ratio.

## CONCLUSIONS

A large amount of subcritical damage occurs during flexural loading of G40-600/PMR-15 cross-ply specimens. Apparent flexural strengths of G40-600/ PMR-15 cross-ply specimens are not reduced by mechanical and thermal cycling if the damage induced does not exceed that which occurs normally
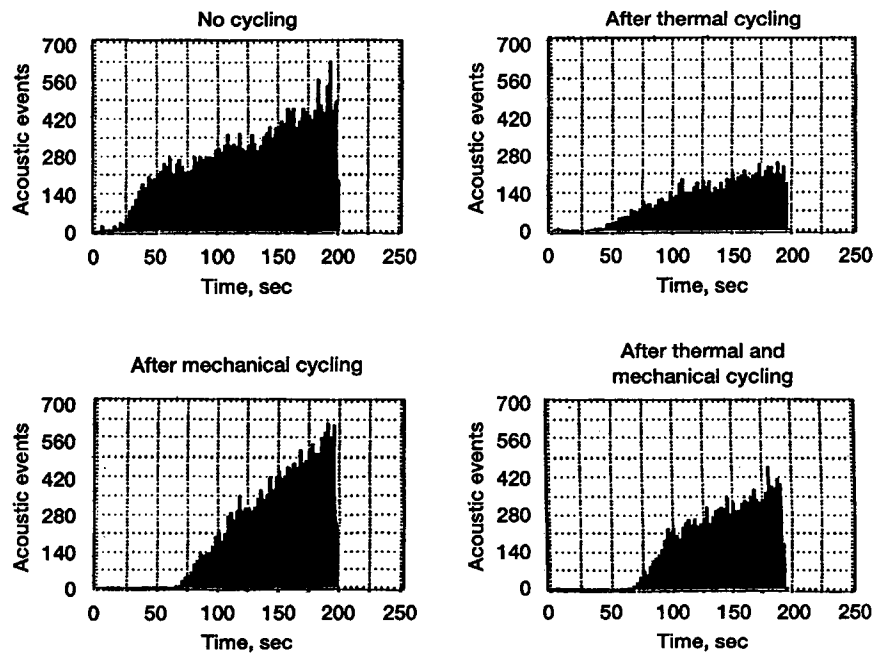


**Figure 11** Effect of low temperature thermal cycling and mechanical cycling on acoustic events recording during four-point bend testing of $(90_2, 0_2)_{2s}$ specimens with a 45/1 span/ depth ratio.
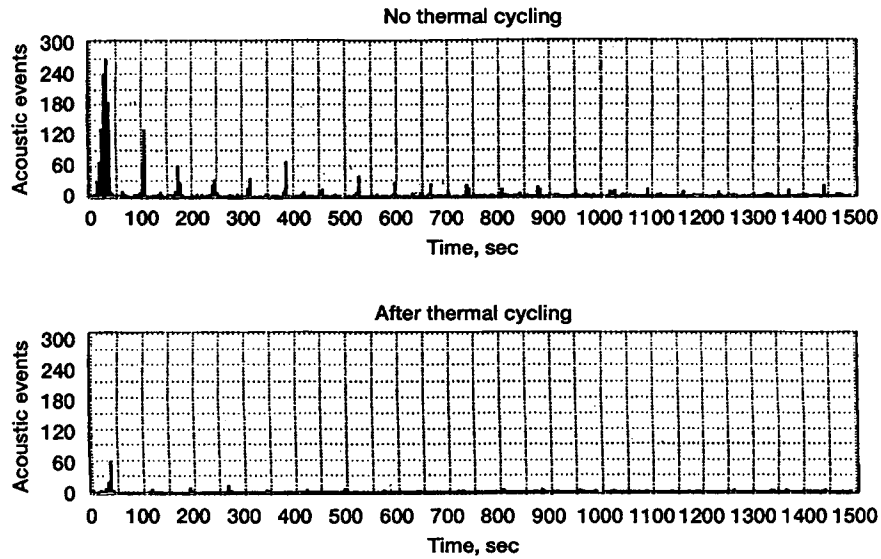
**Figure 12**   Effect of low temperature thermal cycling on acoustic events recorded during subsequent mechanical cycling of $(O_2, 90_2)_{2S}$ specimens tested in four-point bend. (Span/ depth ratio = 45/1. Maximum load = 50% of the failure load.)

during the flexural test. As a result, flexural strength measurements alone provide little information about the damage induced by thermal and mechanical fatigue. The onset of damage during flexural testing can be easily detected by monitoring acoustic emission with a single detector. Two detectors can be used to determine the location of subcritical damage that occurs at various strains during the flexural

test. Further work is needed to determine the types of failure associated with particular acoustic events. More extensive testing of mechanical properties would be required to determine whether or not the damage caused by thermal and mechanical fatigue could be tolerated in a particular application. However, the flexural test data indicate that a substantial amount of damage may be tolerated in applications
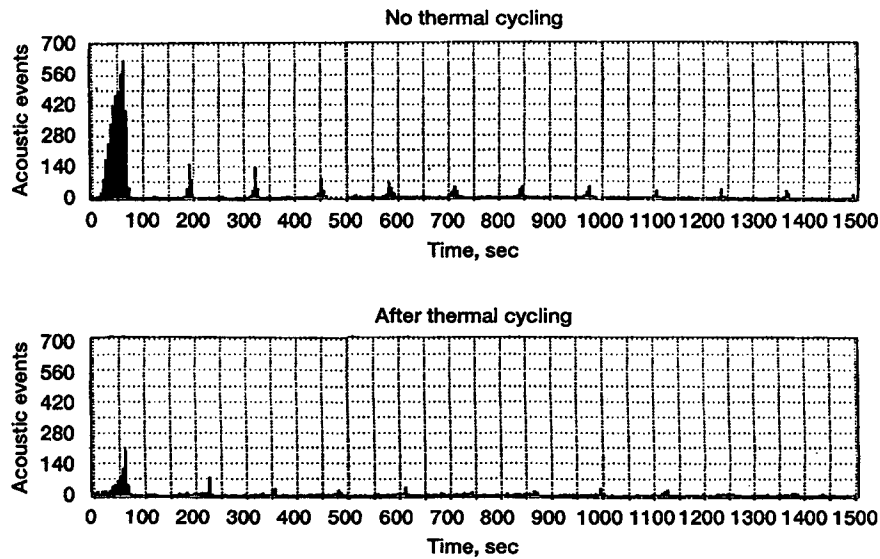


**Figure 13**   Effect of low temperature thermal cycling on acoustic events recorded during subsequent mechanical cycling of $(90_2, O_2)_{2S}$ specimens tested in four-point bend. (Span/ depth ratio = 45/1. Maximum load = 50% of the failure load.)

for which flexural strength is the primary design consideration. This could include some applications for satellites in low Earth orbit, but only if the adverse effects of damage on compressive strength, modulus, and coefficient of thermal expansion could be tolerated. For high temperature aeronautics applications, the reduced compressive strength and the accelerated rate of oxidative degradation caused by microcracking are critical issues. For these applications, acoustic emission measurements provide useful information about the growth of damage during thermal cycling. The feasibility of measuring acoustic emission at higher temperatures and during thermal cycling should therefore be considered.

## REFERENCES

1. J. Awerbuch, W. F. Eckles, and D. L. Erdman, Detection of Failure in Cross-Ply Graphite/Epoxy During Fatigue Loading Through Acoustic Emission, Air Force Report WRDC-TR-89-3087-Vol. 1 (1989).
2. K. Ono, in Proc. 2nd Internat. Symp. Acoustic Emission Reinforced Plast., CARP/Society of Plastics Industry, New York, 1986, pp. 22–28. also *J. Reinforced Plast.*, **7**, 90 (1988).
3. H. Otsuka, *J. Composite Mater.*, **5**, 591 (1981).
4. N. Sato, T. Kurauchi, and O. Kamigaito, *J. Mater. Sci.*, **21**, 1005 (1986).
5. D. G. Zimcik, D. Prouix, C. Roy, and A. Maslouhi, in *The Nation's Future Materials Needs, 19th International SAMPE Technical Conference*, SAMPE, Covina, CA, 1987, pp. 360–371.
6. Test Methods for Flexural Properties of Unreinforced and Reinforced Plastics and Electrical Insulating Materials, ASTM Standard D 790-91.
7. Test Method for Apparent Interlaminar Shear Strength of Parallel Fiber Composites by Short Beam Method, ASTM D 2344-84 (1989).
8. J. M. Whitney, C. E. Browning, and A. Mair, in Composite Materials: Testing and Design (Third Conference), ASTM STP-546, ASTM, Philadelphia, PA, 1974, pp. 30–45.
9. J. M. Whitney, in *Interlaminar Response of Composite Materials*, N. J. Pagano, Ed., Elsevier, New York, 1989, pp. 161–250.
10. S. S. Tompkins and S. L. Williams, in AIAA/ASME/ ASCI/AMS 23rd Structural Dynamics and Materials Conference, AIAA, New York, 1982, pp. 239–246.
11. S. W. Tsai, *Composites Design*, 4th ed., Think Composites, Dayton, OH, 1988.